Roton excitations of the hydrogen molecule in the $Ar(H_2)_2$ compound

Francesco Grazzi,[1,3,4,*] Mario Santoro,[3,4,†] Massimo Moraldi,[1,3,‡] and Lorenzo Ulivi[2,3,4,§]
[1]*Dipartimento di Fisica, Università di Firenze, via G. Sansone 1, I-50019 Sesto Fiorentino, Italy*
[2]*IFAC–CNR, via Panciatichi 56/30, I-50127 Firenze, Italy*
[3]*INFM, Unità di Firenze, Via Giovanni Sansone 1, I-50019 Sesto Fiorentino, Italy*
[4]*LENS, Via Nello Carrara 1, I-50019 Sesto Fiorentino, Italy*
(Received 26 April 2002; published 14 October 2002)

In the $Ar(H_2)_2$ stoichiometric compound, stable only at high pressure, the $S_0(0)$ rotational excitation shows a complicated fine structure when the ortho-H_2 concentration is sufficiently low in the sample. In this work experimental results for the rotational frequencies are reported up to 70 GPa. Moreover, we present here the details of the theoretical analysis, by which we calculate the number of active Raman rotational components, their symmetries, relative intensities, and shifts from the unperturbed rotational frequency, on the basis of the known models for the H_2-H_2 and H_2-Ar anisotropic interaction. The calculated frequencies are extremely sensitive to the shape of the anisotropic interaction potential components, and agree with the measured ones, up to 35 GPa, only if some adjustments are done on the literature models, especially for small intermolecular distances. All the newly determined anisotropic H_2–H_2 and H_2–Ar interaction potential components are reported and compared with literature values.

DOI: 10.1103/PhysRevB.66.144303 PACS number(s): 62.50.+p, 78.30.−j, 34.20.Gj

I. INTRODUCTION

The study of molecular solids, and of solid hydrogen in particular, has gained great benefit from spectroscopic results, which have contributed, more than any other technique, to the understanding of the structural and dynamical properties.[1,2] Spectroscopic data have an even greater importance in high pressure studies, where other direct techniques (neutrons, x rays) encounter difficulties either for the sample dimensions or for the weakness of the scattered signal. Hydrogens under pressure have attracted a great interest in the past years, triggered by the prediction of the pressure-induced transition to a metal state. A large amount of spectroscopic studies, though failing to demonstrate the metallization, have revealed many unexpected phenomena at high pressure, evidencing progressive changes in the intermolecular interactions.[2]

Stoichiometric compounds containing molecular hydrogen as one of the components also have great importance for studying the properties and the interactions of the hydrogen molecule in this environment. A recent study, by infrared spectroscopy, of $Ar(H_2)_2$ has revealed strong analogies between the dynamical behavior of the H_2 molecules in this compound and in solid H_2, at least up to 50 GPa.[3] In particular, the molecules rotate almost freely in both cases, and their interaction gives rise to a vibrational coupling effect, which is described quantitatively by the same model. Also the intrinsic ortho-para conversion rate in a solid sample of $Ar(H_2)_2$ grows very rapidly with pressure[4] much like in solid H_2.[5] It is then possible, in a reasonable time, to obtain a sample with an almost complete para-H_2 proportion [para-$Ar(H_2)_2$], by keeping the sample at cryogenic temperature.

In solid hydrogen, when the concentration of the ortho-H_2 is sufficiently low, even the fine details of the spectra can be modeled from first principles. This analysis has been particularly fruitful for determining the structural properties of the solid. As an example, it suffices to mention the demonstration of the hexagonal close packed (hcp) structure of the solid, by the observation of the splitting of the pure rotational molecular $S_0(0)$ line into a triplet.[6] Analogously, the spectroscopic properties of para-$Ar(H_2)_2$ reflect with great sensitivity all the details of the structure and of the interaction among molecules, and the absence of ortho-H_2 in the sample makes the theoretical analysis much easier.

We have recently reported some experimental results on the pure rotational Raman band $S_0(0)$ of the H_2 molecule in para-$Ar(H_2)_2$.[7] The observed pressure evolution of the fine structure has been modeled on the basis of a theoretical analysis. The comparison between experimental results and calculation has demonstrated that these data can serve for a reliable determination of the anisotropic intermolecular potential in the solid for H_2-H_2 and H_2-Ar at short range. In this paper we present all the experimental data and discuss some specific aspect of the experiment, and, principally, the theory in detail. This is carried out for a rigid lattice on the basis of perturbation theory,[6] with pair additive anisotropic components of the H_2-Ar and H_2-H_2 potentials. A good agreement with the experiment is obtained with potential functions different from those given in the literature, mostly in the short-range repulsive core. Here we report all the newly determined potential components.

This paper is organized as follows. In Sec. II, we will describe the experiment and show the results. Section III is devoted to a thorough explanation of the theory and of the approximations involved. In Sec. IV we discuss the shape of the interaction potential components, and present our conclusions.

II. EXPERIMENT

An Ar/H_2 mixture in stochiometric 1:2 proportion solidifies at about 4.3 GPa at room temperature, and forms the $Ar(H_2)_2$ compound, whose structure has been studied by synchrotron x-ray diffraction.[8] Recent spectroscopic results[3]

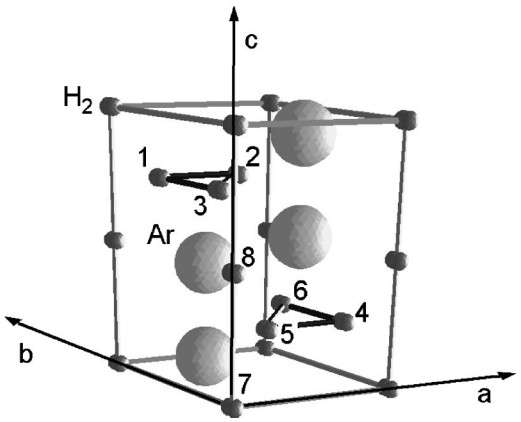

FIG. 1. Crystallographic unit cell of the $Ar(H_2)_2$ compound. The eight hydrogen molecules are labeled with numbers from 1 to 8 to write explicit expression for the wave functions in Sec. III A.

are consistent with the structure proposed after the diffraction experiment, that is, space group D_{6h}^4 ($P6_3/mmc$) with eight H_2 molecules and four Ar atoms in the unit cell. A drawing of the unit cell is reported in Fig. 1, where the H_2 molecules are identified with numbers from 1 to 8. This is necessary to write explicit expressions for the wave functions (see Sec. III A). The coordinates of the Ar atoms and of the molecular centers of mass in the unit cell are given explicitly in Ref. 3.

A diamond anvil cell (DAC) was filled with the gas mixture at about 1000 bar and room temperature. One or more ruby chips, inside the sample region, served to measure internal pressure.[9] We used a Cu-Be gasket for experiments up to 36 GPa and a rhenium gasket for higher pressures. A single crystal of $Ar(H_2)_2$ was grown by slowly rising pressure at room temperature. In all our samples, as it often happens for this compound, the solid has grown with the crystallographic c-axis along the cell axis, as seen observing the faceted (hexagonal) crystal during the growth process. The DAC is then mounted on the cold finger of a close-cycle cryostat. We employed a forward scattering configuration, using either the 488.0- or 514.5-nm line of an Ar^+ laser. The incident radiation is focused into a spot of about 10μm diameter on the sample by a microscope objective (Nikon 20× SLWD) and the scattered radiation is collected by an equal objective, in a confocal configuration. Both objectives are inside the cryostat vacuum chamber but their position can be controlled externally. The radiation is analyzed by an U-1000 Jobin-Yvon or a Spex Triplemate spectrometer, both equipped with a CCD detector cooled with liquid nitrogen. We use a notch filter positioned in front of the entrance slit to prevent the radiation at the laser frequency to enter the monochromator.

When the pressurized sample is cooled to cryogenic temperatures (around 30 K), conversion of H_2 molecules from the ortho species to the para one takes up at a rate which is strongly pressure dependent.[4] In order to measure the ortho-para concentration, we recorded spectra in the frequency region from 150 to 800 cm^{-1}, where the pure rotational transitions of the hydrogen molecule give rise to the $S_0(0)$ and $S_0(1)$ bands. One then observes the progressive decrease of

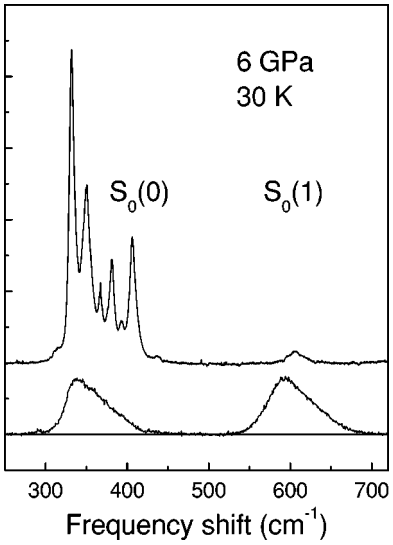

FIG. 2. Shape of the $S_0(0)$ and $S_0(1)$ hydrogen rotational bands before and after ortho-para conversion, at a pressure of about 6 GPa and a temperature of 30 K. The $S_0(0)$ band shows a complicated internal structure which becomes clearer as conversion proceeds.

the intensity of the $S_0(1)$ band with time and the progressive structuring of the $S_0(0)$ band. Only when conversion is almost complete the $S_0(0)$ band develops a complicated fine structure, showing several peaks. In Fig. 2 we present two spectra in the frequency region relative to the rotational transitions $S_0(0)$ and $S_0(1)$, collected at the same pressure and temperature of 6 GPa and 30 K, with a time interval of about 300 h. The lower curve corresponds to the sample just after cooling, which presents a substantial concentration of ortho-H_2 molecules, while the upper spectrum, where the ortho-H_2 concentration is as low as 3%, shows the fine structure of the $S_0(0)$ line. At this pressure, the $S_0(0)$ band spreads over a frequency range of about 100 cm^{-1}. Five components with larger intensity are evident, while some weaker components create several shoulders.

With completely converted samples ($\simeq$3% ortho-H_2) at about 30 K, we have measured spectra along several isothermal pressure scans up to 68 GPa. With increasing pressure, the total frequency spread of the $S_0(0)$ band increases from 80 cm^{-1} at 4 GPa to 250 cm^{-1} at 68 GPa. The various components also change their relative intensity. At 14 GPa a peak enters into the investigated frequency range, from the low frequency side, and moves rapidly with pressure toward higher frequencies, being located at 210 cm^{-1} at 16 GPa and at 250 cm^{-1} at 26 GPa. Due to its evolution with pressure, we assign this line to a lattice phonon excitation. At 35 GPa it overlaps a weak component of the $S_0(0)$ band, showing interesting hybridization phenomena, and then it overlaps and eventually goes beyond the most intense component of the $S_0(0)$ band, producing substantial changes on the shape of the band.

Polarization analysis has been essential to assign the various peaks of the band to the computed active components. This in principle is possible, knowing the orientation of the crystal, but encounters serious experimental difficulties due to the depolarization of the radiation by the two stressed

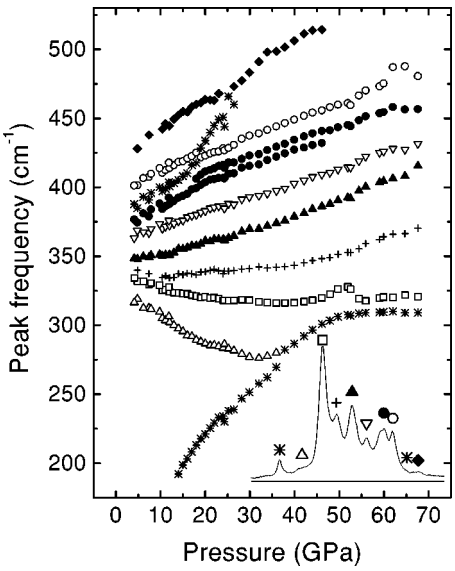

FIG. 3. Pressure behavior of the frequencies of the measured peaks. Full and empty symbols represent assigned $S_0(0)$ components, polarized and not polarized, respectively. Asterisks represent bands with a large pressure slope, that are tentatively assigned to lattice phonons. Phonon-roton interactions are evident at pressures where resonance occurs. The position of a weak band which is not assigned is represented with crosses. A typical spectrum at about 30 GPa is reported in the inset to show the assignment.

diamonds. Observing the vibron Raman line of the H_2 molecules around 4150 cm^{-1}, with the use of a Babinet-Soleil compensator and of a polarizer after the DAC, we have obtained a substantial contrast between two perpendicularly polarized components of the scattered intensity. The configuration for which the measured vibron intensity is a minimum would correspond, without scrambling effects of the diamonds, to vertically polarized incident radiation and horizontally polarized scattered radiation (VH configuration). Spectra measured in this configuration and with the polarizer rotated by 90 degrees (VV configuration) demonstrate different polarization for different components (see Fig. 2 of Ref. 7).

A fit procedure of the fine structure, performed by means of pseudo-Voigt line shapes, has allowed us to obtain the value of the line positions, intensities and widths for every pressure. In Fig. 3 we report the frequency position of the $S_0(0)$ components up to the maximum pressure reached in this work. There are at least eight lines for all pressure values even if at higher pressures it is difficult to determine the weaker ones.

The frequency positions of the maxima of the components increases slowly with pressure, and the total spread of the band increases substantially. Its *center of mass* moves very little due to the weak pressure dependence of the most intense peak. Two peaks with a much higher slope than the average one are assigned to lattice phonon excitations. These are marked with an asterisk in Fig. 3. Interesting hybridization phenomena occur at pressures where such phonon lines are almost resonant with a rotational excitation of the same symmetry. Such crossings are evident around 40 GPa at low energy, and between 20 and 30 GPa at higher energy. The latter phonon band becomes very weak when its frequency grows higher than the upper limit of the $S_0(0)$ band.

The relative displacement of the energy levels is a consequence of the intermolecular interactions, which create a strong perturbation into the $J=2$ manifold. Their measurement can provide deep insight into the properties of this quantum solid. This effect will be calculated in the next section, in the framework of a first order perturbation theory.

III. THEORY

A. Raman active transitions

In this section we evaluate the energies of the rotational $S_0(0)$ states, using a method that is taken from Ref. 6 and extended here to the case of $Ar(H_2)_2$. In such a method the rotational motion of the molecules is treated perturbatively with respect to the anisotropic components of the intermolecular potential. At zeroth order the intermolecular interactions are thus purely isotropic and the molecules rotate freely. The anisotropic components of the interactions are taken into account at first order with the consequence that the rotational quantum number J is still a good quantum number.

We consider a rigid $Ar(H_2)_2$ lattice for what concerns Ar and H_2 centers of mass. Also the H_2 molecular bond is assumed to be rigid. We refer to Fig. 1 for the positions and numbering of the atoms and molecules in the primitive cell.

The rotational states that can be Raman excited from the $J=0$ ground state can be represented by $\mathbf{k}=0$ Bloch waves. That is due to the fact that the exciting radiation is in the visible and thus, for all practical purposes, its linear momentum can be neglected. In view of the previous consideration we write the wave function for the $J=2$ rotational states that can be Raman excited as

$$\psi=\frac{1}{\sqrt{N(4\pi)^{8N-1}}}\sum_{q=1}^{N}\sum_{p=1}^{8}\sum_{m=-2}^{+2}C_{pm}Y_{2m}(\Omega_{qp}). \quad (1)$$

Here the index q runs over all the primitive cells of the system, p indicates one H_2 molecule in the qth primitive cell, and Ω_{qp} represents its orientation in a laboratory frame having the z axis along the crystallografic c axis. $Y_{2m}(\Omega)$ are spherical harmonics and C_{pm} are appropriate coefficients. The normalization of the ψ functions leads to the condition

$$\sum_{p=1}^{8}\sum_{m=-2}^{+2}|C_{pm}|^2=1.$$

There are 40 linearly independent ψ functions due to the eight H_2 molecules present in the cell and to the five possible m values for the projection of the molecular angular momentum. The energies of the $\mathbf{k}=0$ rotational states could thus be obtained by diagonalizing a 40×40 matrix.

Calculations are simpler if the functions ψ are chosen among those that transform according to the irreducible representations of the rotation group of the crystal.[10] The symmetry group for rotations is D_{6h}. It contains six g irreducible representations (A_{1g}, A_{2g}, B_{1g}, B_{2g}, E_{1g}, and E_{2g}) and

six similar u representations. A Raman transition from the ground to the $J=2$ rotational band is possible only if

$$\langle 0|\alpha_\mu|\psi\rangle \neq 0,$$

where $|0\rangle$ represents the ground rotational state of the crystal. The quantity α_μ is the μth spherical component of the anisotropic part of the polarizability (the isotropic, or trace, component does not contribute to the excitation of the $J=2$ state).[6] Because the $|0\rangle$ state transforms as A_{1g}, only the $|\psi\rangle$ states that transform according to the irreducible transformations contained in α_μ can be Raman excited.

Since the spherical components of the polarizability α_0, $\alpha_{\pm 1}$, and $\alpha_{\pm 2}$ transform, respectively, as A_{1g}, E_{1g}, and E_{2g}, it is sufficient to consider only those ψ functions that transform according to these representations. By the application of standard methods of group theory[10] it can be shown that the (reducible) representation of the rotation group, whose basis is given by the ψ functions of Eq. (1), contains three times the representation A_{1g}, four times E_{1g}, and five times E_{2g}.

We write down explicitly convenient basis functions for those irreducible representations and, to this aim, first define the auxiliary functions

$$\begin{aligned} X^q_\mu(\Omega_{q1},\ldots,\Omega_{q6}) &= \sum_{p=1}^{6} Y_{2\mu}(\Omega_{qp}), \\ Z^q_\mu(\Omega_{q1},\ldots,\Omega_{q6}) &= \sum_{p=1}^{6} Y_{2\mu}(\Omega_{qp})\chi^{2(p-5)} \end{aligned} \tag{2}$$

with $\chi=\exp(2\pi i/6)$. By means of the previous definitions we can write the basis functions for the three irreducible representations A_{1g}:

$$\begin{aligned} \psi^{(1)}_{A_{1g}} &= A\sum_{q=1}^{N} [Y_{20}(\Omega_{q7})+Y_{20}(\Omega_{q8})]/\sqrt{2}, \\ \psi^{(2)}_{A_{1g}} &= A\sum_{q=1}^{N} X^q_0(\Omega_{q1},\ldots,\Omega_{q6})/\sqrt{6}, \\ \psi^{(3)}_{A_{1g}} &= A\sum_{q=1}^{N} [Z^q_2(\Omega_{q1},\ldots,\Omega_{q6}) \\ &\quad + \chi^2 Z^{q*}_2(\Omega_{q1},\ldots,\Omega_{q6})]/\sqrt{12}; \end{aligned} \tag{3}$$

for the four representations E_{1g}:

$$\begin{aligned} \psi^{(1)}_{E_{1g}} &= A\sum_{q=1}^{N} \frac{1}{\sqrt{2}}\times\begin{pmatrix} Y_{21}(\Omega_{q7})+Y_{21}(\Omega_{q8}) \\ Y^*_{21}(\Omega_{q7})+Y^*_{21}(\Omega_{q8}) \end{pmatrix}, \\ \psi^{(2)}_{E_{1g}} &= A\sum_{q=1}^{N} \frac{1}{\sqrt{6}}\times\begin{pmatrix} X^q_1(\Omega_{q1},\ldots,\Omega_{q6}) \\ X^{q*}_1(\Omega_{q1},\ldots,\Omega_{q6}) \end{pmatrix}, \\ \psi^{(3)}_{E_{1g}} &= A\sum_{q=1}^{N} \frac{1}{\sqrt{6}}\times\begin{pmatrix} Z^{q*}_1(\Omega_{q1},\ldots,\Omega_{q6}) \\ Z^q_1(\Omega_{q1},\ldots,\Omega_{q6}) \end{pmatrix}, \\ \psi^{(4)}_{E_{1g}} &= A\sum_{q=1}^{N} \frac{1}{\sqrt{2}}\times\begin{pmatrix} Y^*_{22}(\Omega_{q7})-Y^*_{22}(\Omega_{q8}) \\ Y_{22}(\Omega_{q7})-Y_{22}(\Omega_{q8}) \end{pmatrix}; \end{aligned} \tag{4}$$

and for the five representations E_{2g}:

$$\begin{aligned} \psi^{(1)}_{E_{2g}} &= A\sum_{q=1}^{N} \frac{1}{\sqrt{2}}\times\begin{pmatrix} Y_{22}(\Omega_{q7})+Y_{22}(\Omega_{q8}) \\ Y^*_{22}(\Omega_{q7})+Y^*_{22}(\Omega_{q8}) \end{pmatrix}, \\ \psi^{(2)}_{E_{2g}} &= A\sum_{q=1}^{N} \frac{1}{\sqrt{6}}\times\begin{pmatrix} Z^{q*}_0(\Omega_{q1},\ldots,\Omega_{q6}) \\ Z^q_0(\Omega_{q1},\ldots,\Omega_{q6}) \end{pmatrix}, \\ \psi^{(3)}_{E_{2g}} &= A\sum_{q=1}^{N} \frac{1}{\sqrt{6}}\times\begin{pmatrix} X^q_2(\Omega_{q1},\ldots,\Omega_{q6}) \\ X^{q*}_2(\Omega_{q1},\ldots,\Omega_{q6}), \end{pmatrix}, \\ \psi^{(4)}_{E_{2g}} &= A\sum_{q=1}^{N} \frac{1}{\sqrt{6}}\times\begin{pmatrix} Z^{q*}_2(\Omega_{q1},\ldots,\Omega_{q6}) \\ Z^q_2(\Omega_{q1},\ldots,\Omega_{q6}) \end{pmatrix}, \\ \psi^{(5)}_{E_{2g}} &= A\sum_{q=1}^{N} \frac{1}{\sqrt{2}}\times\begin{pmatrix} Y^*_{21}(\Omega_{q7})-Y^*_{21}(\Omega_{q8}) \\ Y_{21}(\Omega_{q7})-Y_{21}(\Omega_{q8}) \end{pmatrix}, \end{aligned} \tag{5}$$

where A is the normalization factor

$$A=\frac{1}{\sqrt{N(4\pi)^{8N-1}}}.$$

The zeroth order eigenstates and first order eigenvalues for the rotational motion are then obtained by diagonalizing the anisotropic potential energy V for states of the same symmetry:

$$V_{ij}(\Gamma\gamma)=\langle\psi^{(i)}_{\Gamma\gamma}|V|\psi^{(j)}_{\Gamma\gamma}\rangle, \tag{6}$$

where Γ stands for one of the three irreducible representations (A_{1g},E_{1g},E_{2g}), and γ specifies the line in case the representation is not unidimensional (E representations). In the case of E representations, however, the two basis functions are complex conjugates of one another, which makes them equivalent for our purposes. The rotational states associated with an E representation are doubly degenerate.

One further simplification arises from the fact that the anisotropy of the intermolecular potential does not mix $\psi^{(4)}_{E_{1g}}$ and $\psi^{(5)}_{E_{2g}}$ with the other functions of the same symmetry, so that the matrices to diagonalize have dimensions 3×3 for E_{1g} and 4×4 for E_{2g}. Moreover, the states represented by $\psi^{(4)}_{E_{1g}}$ and $\psi^{(5)}_{E_{2g}}$ are not Raman active, because they have magnetic quantum numbers (± 2 and ± 1, respectively) that do not match the μ values of the polarizability components needed for the transitions to those states (± 1 and ± 2, respectively).

In the end we are left with ten $\mathbf{k}=0$ levels corresponding to Raman active states: three of A_{1g} symmetry, three (doubly degenerate) of E_{1g} symmetry, and four (doubly degenerate) of E_{2g} symmetry.

B. Polarization

As described in Sec. II, our scattering geometry is such that the crystal symmetry axis is aligned with the light wave vector and the scattered light is observed along the same direction, so that we collect mostly the components xx and xy. The relations between spherical and orthogonal components of the anisotropy of the polarizability are

$$\alpha_{xx} \propto \alpha_2 + \alpha_{-2} - \sqrt{\frac{2}{3}}\alpha_0,$$
$$\alpha_{xy} \propto \alpha_2 - \alpha_{-2}. \tag{7}$$

From their symmetry, it is readily seen that the polarizability components transform as A_{1g} and E_{2g}. It is thus expected that the lines associated with the E_{1g} states are absent, or very weak, in the experimental spectrum which thus contains essentially the components associated to the three A_{1g} energies and to the four (doubly degenerate) E_{2g} energies. It is also seen that α_{xx} contains both A_{1g} and E_{2g}, while α_{xy} contains only E_{2g}, which is a consequence of the fact that A_{1g} states are fully polarized.

For the calculation of the Raman line intensities, matrix elements as in Eq. (6) have to be calculated. In order to do this we assume that the polarizability is composed only of single molecule contributions

$$\alpha_\mu \propto \beta \sum_{q=1}^{N} \sum_{p=1}^{8} Y_{2\mu}(\Omega_{qp}), \tag{8}$$

where β is the polarizability anisotropy of the single hydrogen molecule.

C. Intermolecular interactions

For the calculation of the energy of the rotational states we need a model for the anisotropic potential energy V. We assume that V is pairwise additive, that is,

$$V = \frac{1}{2} \sum_{ij} v_{ij}^{(H_2-H_2)} + \sum_{ik} v_{ik}^{(H_2-Ar)}, \tag{9}$$

where now i and j enumerate the hydrogens and k the argons in the whole crystal. The pair intermolecular potential functions v are expanded in spherical components in the usual way, that is

$$v_{ij} = (4\pi)^{3/2} \sum_{l_1 l_2 L} V_{l_1 l_2 L}(R_{ij}) F_{l_1 l_2 L}(\Omega_i, \Omega_j, \Omega_{ij}), \tag{10}$$

where the function $F_{l_1 l_2 L}$ (with $l_1, l_2, L \neq 0,0,0$) takes into account the dependence from the angular coordinates of the ith and jth molecules (Ω_i and Ω_j) and of the vector joining them (Ω_{ij}). For H_2-Ar interaction, $l_2 = 0$. The function $F_{l_1 l_2 L}$ is given by

$$F_{l_1 l_2 L}(\Omega_1, \Omega_2, \Omega) = \sum_{m_1 m_2 M} Y_{l_1}^{m_1}(\Omega_1) Y_{l_2}^{m_2}(\Omega_2) Y_L^{M*}(\Omega) \times C(l_1 l_2 L; m_1 m_2 M), \tag{11}$$

where $C(l_1 l_2 L; m_1 m_2 M)$ are Clebsh-Gordan coefficients.

For H_2-Ar pairs, information on the anisotropic interaction energy $v^{H_2\text{-}Ar}$ is available in the literature.[11,12] The proposed functional models are fitted on experimental data of rotationally inelastic scattering of molecular beams and of spectroscopy of dimers. In this case, the only reported component is V_{202}. For H_2-H_2 various semiempirical analytic expressions have been derived based on molecular beam scattering data[13,14] and the low temperature second virial coefficient.[14] Moreover a recent theoretical determination is available.[15] For H_2-H_2 we will consider the components $V_{202} = V_{022}$, responsible for crystal field effects, and V_{224}, which gives rise to propagating rotonic excitations. Other components, like V_{222} and V_{220}, are shown to give a negligible contribution.

Analytic functions often used in the past to represent these potential components[11,13] may be written in the general form

$$V(R) = V_{rep}(R) - D(R)[C_6/R^6 + C_8/R^8 + C_{10}/R^{10}], \tag{12}$$

where $V_{rep}(R)$ is a short range repulsive contribution and $D(R)$ is a damping function. More explicitly, for the 202 components of H_2-Ar (Ref. 11) and H_2-H_2,[13] the potential is of the Buckingham-Corner type, that is,

$$V_{rep}(R) = A \exp(-\beta R) \tag{13}$$

and

$$D(R) = \exp(-a(R_0/R - 1)^c) \quad \text{for} \quad R \leqslant R_0$$
$$D(R) = 1 \quad \text{for} \quad R \geqslant R_0. \tag{14}$$

For the 224 component of the H_2-H_2 interaction, $V_{rep}(R)$ is given by[13]

$$V_{rep}(R) = C_5/R^5 + C_7/R^7 \tag{15}$$

and $D(R)$ is the same as in Eq. 14.

IV. RESULTS AND DISCUSSION

The theory described in Sec. III predicts ten allowed Raman transitions. Three of them have zero intensity when the directions of both the incident and scattered radiation coincide with the c axis of the crystal. Among the remaining seven components, three are polarized (A_{1g}) while the other four are not polarized (E_{2g}).

The theory gives the frequency splitting of the $S_0(0)$ features, by the numerical evaluation of the matrix elements as in Eq. (6), and the relative intensities. By the use of Eqs. (2)–(5) for ψ functions and of the equations of Sec. III C for the anisotropic intermolecular potential, each matrix element in Eq. (6) can be written as a lattice sum. The density, and thus the intermolecular distance, has been derived at each pressure using the $Ar(H_2)_2$ equation of state determined by x-ray diffraction.[16] The lattice sum has been calculated by considering, given an H_2 molecule, all its neighbors contained in the closest five primitive cells in each direction. We have verified this to be sufficient for our purposes. Finally,

for each irreducible representation, the diagonalization is easily performed, allowing a determination of the energy corrections and eigenfunctions.

The calculation performed with the anisotropic interaction potential components reported in Refs. 11–15 gives, on the average, a much smaller separation of the lines than the experimental one. We have then adjusted the potential parameters of the model functions for the V_{202}, V_{224} (H_2-H_2) and V_{202} (H_2-Ar) components, performing a best fit of the experimental spectrum.[7] We have limited this analysis to pressures below 35 GPa, because it is to be expected that the perturbative method fails when the distance between nearest neighbors is too short. Our calculations show that the theoretical frequencies change dramatically even for a very small change in the potential model, proving the sensitivity of this method for determining the fine details of the anisotropic interaction. As a merit parameter to judge of the goodness of the fit, we have chosen, somewhat arbitrarily, the sum of the squares of the differences between the theoretical and experimental frequencies, weighted with the corresponding intensities. An alternative method we have exploited was to calculate a theoretical spectrum, choosing a linewidth for each component, and comparing it with the spectrum obtained from the experimental frequency positions and intensities, using the same linewidths. In both cases, the experimental and theoretical frequencies of the most intense component have been set equal, since the theory provides only the shifts from the unperturbed rotational frequency. The comparison between experimental and calculated frequencies has been already presented (see Fig. 3 of Ref. 7) and is satisfactory for most of the components, with the exception of the two extreme lines. For these ones the perturbative correction is quite large, and may not be correctly accounted for by the first order theory. In Fig. 4 we report a comparison of the overall computed (right panel) and experimental spectra (left panel), after subtraction from these latter of the unassigned components and of the lines assigned to lattice phonons. For the components of the computed spectra we have used the experimentally determined linewidths. The computed peak assigned to the experimental highest frequency mode (solid diamond) is centered above 500 cm^{-1}, and does not appear in the figure. For the most intense components, a good agreement at all pressures is visually evident from the figure. Some discrepancy in the intensity can be detected for some components (e.g., that indicated by upside-down triangles). A better agreement should imply the use of an increased number of free parameters in the potential model, which appears to us not to be justified.

In Figs. 5 and 6 the anisotropic components V_{202} (for H_2-Ar and H_2-H_2) and the component V_{224} (for H_2-H_2) obtained by our fit are reported together with previous models.[11–15] The values of the potential parameters [see Eqs. (12), (13), (14), and (15)] of the V_{202} components, both for H_2-H_2 and for H_2-Ar, are reported in Table I of Ref. 7. For the H_2-H_2 V_{224} component we obtain $C_5=1160$, $C_7=275$ $C_6=194$ $C_8=1250$ $C_{10}=15700$ $a=1.2$, $c=2$, and $R_0=5.82$, for energies measured in cm^{-1} and lengths in Å. The resulting V_{224} component is very similar to the models given in Refs. 13 and 14. Also the V_{202} component for H_2-Ar

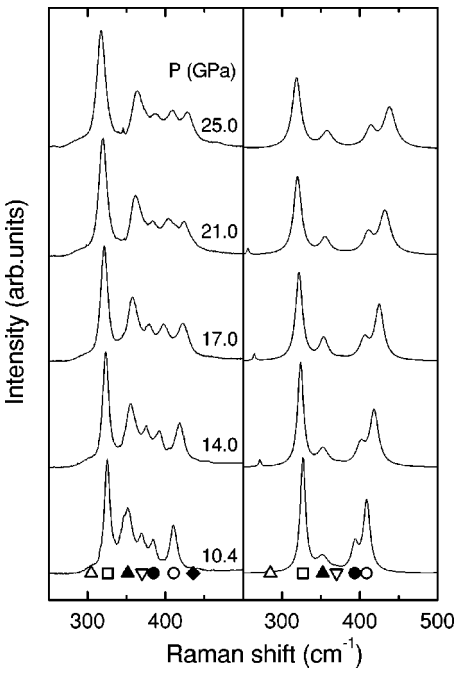

FIG. 4. Left panel: experimental spectra, after having removed the weak unassigned components. Right panel: spectra computed by using, for each theoretical component, a Lorentzian lineshape having the computed frequency and intensity, and a width as close as possible to the experimental one. The symbols mark the position of each component and correspond to the ones used in Fig. 3. No polarization selection has been applied in the measurements in these cases and the spectra have been calculated accordingly.

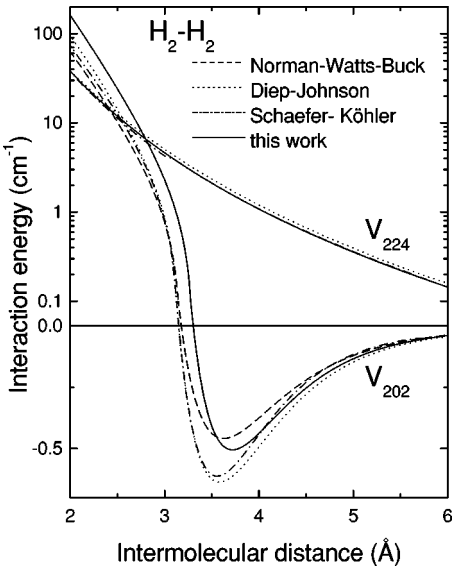

FIG. 5. Anisotropic components of the H_2-H_2 interaction potentials. Dashed, dotted and dash-dotted lines are from Refs. 13–15, while the continuos line is our model. In the case of V_{224} the difference between this latter and the potential of Refs. 13 and 14 is negligible, while it is more substantial for the case of V_{202}, even though in this case also the models reported in the literature do not agree among themselves.

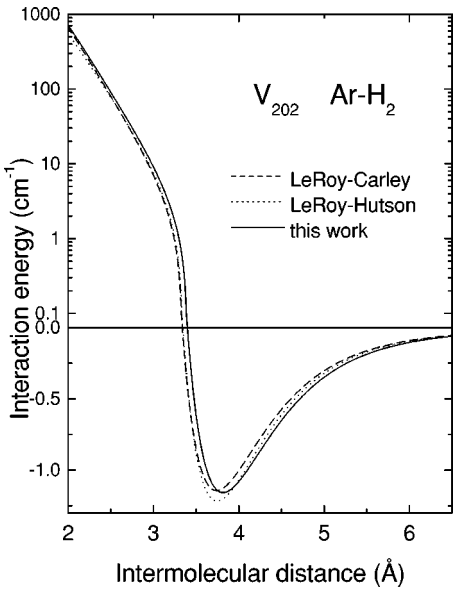

FIG. 6. Anisotropic component of the H_2-Ar interaction potentials. Dashed and dotted lines are from Refs. 11 and 12, while the continuous line is our model.

agrees with previously reported results within a 10% discrepancy. We find, instead, much larger differences for the H_2-H_2 V_{202} component. In the repulsive part, this is almost twice as large as the result of Ref. 13, the difference amounting to about 30–40 cm^{-1} at a distance of 2.5 Å. Such a difference is smaller if one compares either with *ab initio* results of either Ref. 15 or 14 (see Fig. 5).

The discussion on the reliability of our determination of the anisotropic interaction potential has been outlined in Ref. 7. Several approximations are present in the theory, namely, (i) we have neglected the second and the higher orders in the perturbative series; (ii) the molecular centers of mass are considered fixed on a rigid lattice; (iii) only two-body interaction is considered between molecules; and (iv) the 222 anisotropic components of the H_2-H_2 interaction has not been considered in the fitting procedure.

This latest point has little relevance, since V_{222} is very small.[14] We have checked its effect in a few cases, obtaining the result that its inclusion in the calculation of the rotational energy changes this by less than 3%, and its inclusion in the fit procedure does not appreciably changes the calculated potential parameters. The other points are discussed in the following.

(i) The approximation involved in the use of the first order perturbative method has been estimated by computing the second order contribution to the rotational energies coming from the H_2-H_2 and H_2-Ar V_{202} components. This is accomplished rather easily, involving only a crystal field calculation. The result is that the calculated energies change less than 10 cm^{-1} in the pressure range up to 35 GPa. This is also the order of magnitude of the discrepancy with the experimental frequencies. Such a difference, if considered in the potential model fitting, brings forth a quite small change in the potential parameters, that can by no means reduce the discrepancy with the literature models to negligible values.

(ii) The effects related to the zero point motion of the molecular centers of mass, for what concern the quadrupole-quadrupole interaction in H_2-H_2, have been effectively taken into account in the past by the factor ξ_{54}, which reduces the interaction energy by about 5% at the densities of our interest.[17] No similar information is available for the 202 components. It is reasonable, however, to assume that the corrections to be applied to the 202 components are of the same order of magnitude.

(iii) We have used a pair-additive potential for our calculation, without including known dispersion energy coefficients[18] for three body interaction, first because a theory considering also three body potential in the calculation of rotational energy has not been developed, and, in addition, it is not reasonable to use those values at the small intermolecular distances probed by our experiments.

The difference from our determination of the potential components and the literature values can then be understood. As a consequence of (iii), our pair potential may indeed contain effectively many body interactions, and it is appropriate for a dense phase. On the other hand, the potential model obtained by fitting gas phase properties is the sum of a large isotropic part with a much smaller anisotropic part. Therefore, a small variation in the assumed isotropic part of the potential is reflected in a relatively larger variation in the anisotropic components, which may be affected by larger relative uncertainties. This is not the case in our method, because the isotropic potential in a low temperature solid might affect the orientational dynamics only through the small zero point motion. We therefore believe that the results of these kinds of experiments are extremely valuable for a determination of the anisotropic intermolecular interaction, due to the high (and highly selective) sensitivity, even with the limit of being fitted on one property alone.

The knowledge of a reliable, anisotropic empiric pair potential is of paramount importance for a good theoretical description of the high pressure ordered phases of solid H_2.[19,20] This is a quite arduous theoretical problem, to be faced taking fully into account quantum effects in the molecular motion, which are indeed very strong, as is demonstrated by the large difference between H_2 and D_2 transition pressures. Only one quantum mechanical method not demanding for empiric potential models has been reported,[21] but this is affordable only with long runs on big supercomputers, with few molecules. More affordable quantum computations are based on the path integral Monte Carlo method. Such an approach was attempted for hydrogen some time ago,[22] using, however, somewhat arbitrary effective interactions. These were derived on the basis of a comparison with the total energy calculated by density functional theory methods. This procedure to derive an anisotropic interaction potential in the solid testifies to the lack of knowledge about this quantity. We think that the result of our work, deriving anisotropic components of the interaction potential from high density experimental data, is a step towards a modeling of hydrogen ordered phases.

ACKNOWLEDGMENTS

Financial support from the European Union, under the Contract No. LENS HPRICT1999-00111, is gratefully acknowledged.

*Electronic address: grazzi@fi.infn.it
†Electronic address: santoro@lens.unifi.it
‡Electronic address: moraldi@fi.infn.it
§Electronic address: ulivi@ifac.cnr.it

[1] I.F. Silvera, Rev. Mod. Phys. **52**, 393 (1980).
[2] H.K. Mao and R.J. Hemley, Rev. Mod. Phys. **66**, 671 (1994).
[3] L. Ulivi, R. Bini, P. Loubeyre, R. LeToullec, and H.J. Jodl, Phys. Rev. B **60**, 6502 (1999).
[4] F. Grazzi and L. Ulivi, Europhys. Lett. **52**, 564 (2000).
[5] J.H. Eggert, E. Karmon, R.J. Hemley, H.K. Mao, and A.F. Goncharov, Proc. Natl. Acad. Sci. **96**, 12 269 (1999).
[6] J. Van Kranendonk, *Solid Hydrogen* (Plenum Press, New York, 1983).
[7] F. Grazzi, M. Santoro, M. Moraldi, and L. Ulivi, Phys. Rev. Lett. **87**, 125506 (2001).
[8] P. Loubeyre, R. LeToullec, and J.-P. Pinceaux, Phys. Rev. Lett. **72**, 1360 (1994).
[9] H.K. Mao, P.M. Bell, J.V. Shaner, and D.J. Steinberg, J. Appl. Phys. **49**, 3276 (1978).
[10] L. Landau and E. Lifchitz, *Mécanique Quantique* (Mir, Moscow, 1974).
[11] R. J. Le Roy and J. Scott Carley, *Adv. Chem. Phys*, edited by K. P. Lawley (Wiley, NY, 1980), p. 353.
[12] R.J. Le Roy and J.M. Hutson, J. Chem. Phys. **86**, 837 (1987).
[13] M.J. Norman, R.O. Watts, and U. Buck, J. Chem. Phys. **81**, 3500 (1984). Here the original values of C_5 and C_7 for V_{224} are exchanged. Such a modification does not alter the conclusions presented in the present reference [U. Buck, private communication], but reproduces correctly the long-range behavior of the potential.
[14] J. Schaefer and W.E. Koehler, Z. Phys. D: At., Mol. Clusters **13**, 217 (1989).
[15] P. Diep and J.K. Johnson, J. Chem. Phys. **112**, 4465 (2000).
[16] P. Loubeyre (private communication).
[17] V.V. Goldman, Phys. Rev. B **20**, 4478 (1979).
[18] S.A.C. McDowell and W.J. Meath, Mol. Phys. **90**, 713 (1997).
[19] I.F. Silvera and R.J. Wijngaarden, Phys. Rev. Lett. **47**, 39 (1981).
[20] H.E. Lorenzana, I.F. Silvera, and K.A. Goettel, Phys. Rev. Lett. **64**, 1939 (1990).
[21] H. Kitamura, S. Tsuneyuki, T. Ogitsu, and T. Miyake, Nature (London) **404**, 259 (2000).
[22] K.J. Runge, M.P. Surh, C. Mailhiot, and E.L. Pollock, Phys. Rev. Lett. **69**, 3527 (1992).